

# Mobile Translation Systems Generate Genomically Engineered *Escherichia coli* Cells with Improved Growth Phenotypes

Samuel Gowland and Michael C. Jewett\*

Cite This: *ACS Synth. Biol.* 2022, 11, 2969–2978

Read Online

ACCESS |



Metrics &amp; More

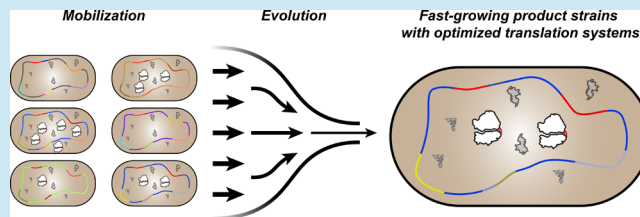


Article Recommendations



Supporting Information

**ABSTRACT:** Cellular translation is responsible for the synthesis of proteins, a highly diverse class of macromolecules that form the basis of biological function. In *Escherichia coli*, harnessing and engineering of the biomolecular components of translation, such as ribosomes, transfer RNAs (tRNAs), and aminoacyl-tRNA synthetases, has led to both biotechnology products and an expanded genetic code. However, the engineering potential of molecular translation is hampered by the limited capabilities for rapidly sampling the large genomic space necessary to evolve well-coordinated synthetic translation networks inside cells. To address this limitation, we developed a genome engineering method inspired by the action of mobile genetic elements termed mobilization. Mobilization utilizes the stochastic action of the recombinase flippase (FLP) to generate up to ~400 million genomic insertions, deletions, or rearrangements at flippase recognition target sites per milliliter of culture per OD in living *E. coli* cells. As a model, we applied our approach to evolve faster-growing *E. coli* strains living exclusively off genomically expressed tethered ribosomes. In an iterative “pulse-passaging scheme,” we generated genomic libraries of cells via induction of FLP recombinase (pulse) followed by passaging the population without induction of FLP to enrich the resulting population for cells with higher fitness. We observed large structural genomic diversity across these cells, with the fastest growing strains exhibiting a 71% increase in growth rate compared to the ancestral strain. We anticipate that both these strains and the mobilization method will be useful tools for synthetic biology efforts to engineer translation systems.



## INTRODUCTION

Molecular translation systems underpin the information flow of the central dogma of biology, enabling the synthesis of sequence-defined polymers of amino acids known as proteins from a specified genetic template. Harnessing and engineering these systems has led to recombinant DNA products (e.g., laundry detergent enzymes) and proteins with diverse genetically encoded chemistry that goes beyond the natural 20 amino acids. For example, recent studies have shown it to be possible to incorporate more than 200 noncanonical amino acids (ncAAs) into proteins cotranslationally.<sup>1–17</sup> Such innovations have led to new biocatalysts,<sup>18</sup> antibody–drug conjugates,<sup>19</sup> and biomaterials.<sup>20</sup>

The advent of genomically recoded *Escherichia coli* organisms<sup>21–26</sup> as well as tethered ribosomes<sup>27–33</sup> represents progress toward engineering individual elements of translation systems for manufacturing proteins with ncAAs. However, translation is a complex process that involves numerous independently expressed factors, including ribosomal RNA (rRNA) and proteins, transfer RNAs (tRNAs), aminoacyl-tRNA synthetases, and initiation, elongation, and release factors. While coordinately tuning and optimizing all of these factors into efficient and stable translation systems is fundamental to all known life forms, mimicking this network efficiency in synthetic translation systems—here including both restructured native translation systems (i.e., synthetic

parts and/or novel expression architectures incorporated into cell-supporting translation networks) and orthogonal translation systems—remains a challenge.<sup>1</sup>

To solve this challenge, a variety of genome engineering tools are available. For example, the Datsenko–Wanner method and CRISPR-Cas-mediated approaches<sup>34,35</sup> can deliver whole gene cassettes onto the genome of *E. coli*.<sup>36</sup> Unfortunately, these approaches typically require a minimum of 1–2 days per edit made in series and are not used for parallel and continuous directed evolution of genomes. In yeast, the SCRaMbLE system has demonstrated more rapid exploration of genomic space than the Datsenko–Wanner method and CRISPR-Cas-mediated approaches.<sup>37–40</sup> The SCRaMbLE system allows rapid generation of millions of structural yeast genome variants in one pot by simple induction of Cre recombinase. However, equivalent recombinase-based techniques to generate massive genomic diversity are underdeveloped for synthetic translation systems in *E. coli*.

Received: February 23, 2022

Published: August 11, 2022



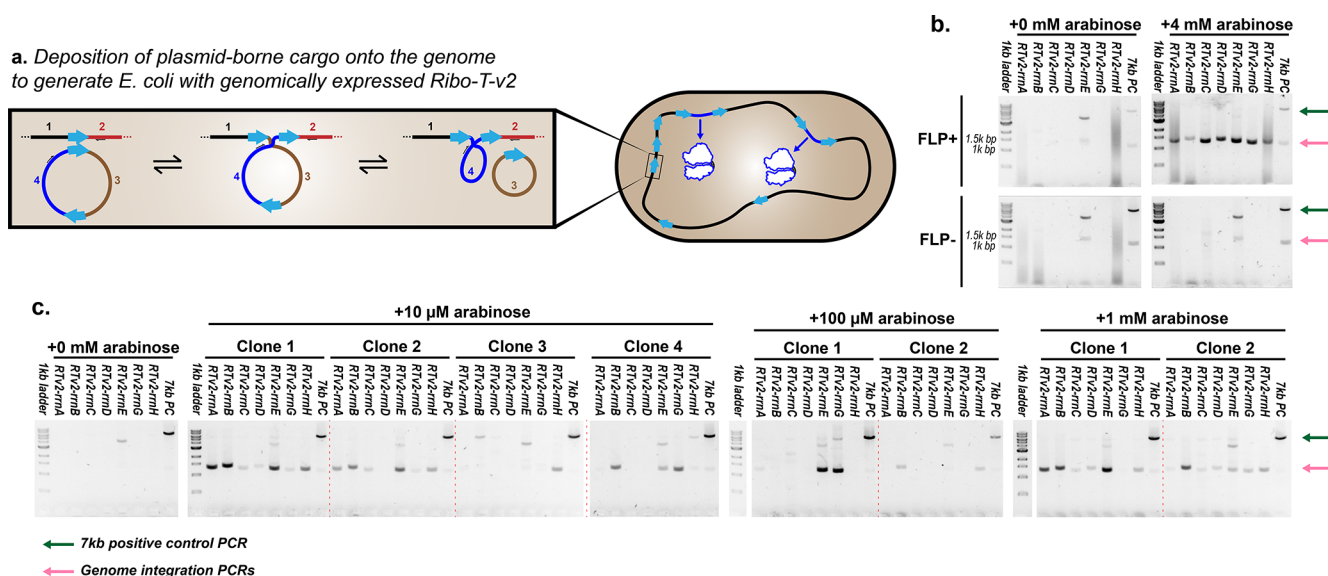


**Figure 1.** FLP-dependent integration of pSLG022 into genomic FRT sites. (a) Circular plasmid (example vector shown in brown; example cargo shown in blue) with two parallel FRT sites may be integrated into the genome, and then the vector can be excised in a two-recombination-step process to allow the integration of desired cargo at FRT sites in the genome. A schematic of an example product strain produced from the mobilization of RTv2 onto the genome of SQ171. Mobilization has introduced two RTv2 cassettes onto the genome to translate the proteome. Small black arrows represent example primer sites for the reactions shown in (b,c). (b) PCR reactions on SQ171(pSLG022, pSLG033) [FLP+] and SQ171(pSLG022, pSLG028) [FLP−] cultures with and without induction by 4 mM arabinose. Approximate expected band sizes for each genomic site assay PCR are shown by the pink arrow and for the 7 kb PCR positive control by the green arrow. Similar results are seen for integration of the plasmid vector, as well as induction by as little as 1 mM arabinose (Figure S1). (c) Characterization of sets of FLP+ clones isolated from the same mobilized populations, with each population grouped by its associated concentration of arabinose induction. As in (b), pink and green arrows signify expected band sizes for the genomic site assay PCR and the 7 kb PCR positive control, respectively. Differing band patterns across the seven genomic FRT sites assayed signifies independent recombinase activity between clones isolated from the same population.

Here, we sought to address this gap by building a platform termed mobilization that allows synthetic biologists to rapidly sample large sets of genome permutations around a small set of specifically targeted gene cassettes. Inspired by the action of mobile genetic elements, which are much more plastic in their copy numbers and expression profiles over evolutionary time than typical genomic elements, we here “mobilize” targeted elements of synthetic translation systems by utilizing flippase (FLP)/flippase recognition target (FRT)-mediated recombination to stochastically recombine FRT-flanked target elements into FRT genomic sites within each cell in a population. We hypothesized that mobilization would allow for rapid exploration and evolution of coordinated expression dynamics of these synthetic translation elements in the context of the native host translation system.

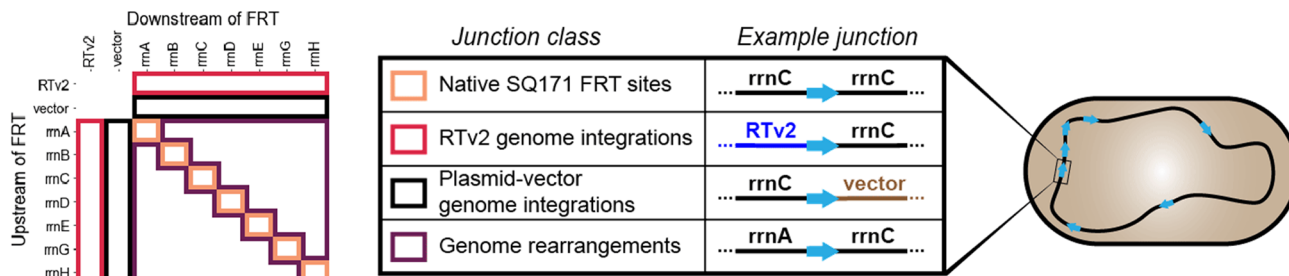
We show that the genomic diversity generated by mobilization can be used to support downstream selections for faster-growing strains via restructuring of the translation system supporting the cell. We apply this platform to transfer cellular dependence in the SQ171 strain of *E. coli*<sup>41</sup> from a plasmid-expressed tethered ribosome, specifically Ribo-T-v2 (RTv2),<sup>31</sup> to a genomically expressed version. Ribo-T-v2 (RTv2)<sup>31</sup> is a ribosome with covalently tethered subunits where core 16S and 23S rRNAs form a single chimeric molecule. We isolated robust chassis strains harboring genomically integrated RTv2 that grow 71% faster than their plasmid-based ancestral strain. Furthermore, we demonstrate that mobilization allows the generation of up to approximately 400 million unique structural rearrangements in living *E. coli* per milliliter per OD of induced culture, allowing for rapid exploration of genomic space. We anticipate that mobilization

will be an important tool that assists future efforts in the construction of complex synthetic translation systems.

## RESULTS AND DISCUSSION

We set out to build a platform for genomic mobilization of synthetic translation systems using FLP/FRT-mediated recombination. First, we asked whether we could transfer cellular dependence in SQ171 from episomally expressed tethered ribosomes (RTv2) to genomically expressed tethered ribosomes (Figure 1a). SQ171 has each of its seven genomic ribosomal operons removed and replaced with an FRT site, thus requiring two plasmids: one expressing the cells’ ribosomes and one expressing essential tRNAs from the deleted ribosomal operons. These two plasmids were exchanged with plasmids that would maintain their essential function while enabling mobilization: the ribosomal plasmid was replaced with a plasmid expressing an RTv2 cassette flanked by two FRT sites on the plasmid vector (pSLG022), and the tRNA plasmid was enlarged to include an arabinose-inducible FLP recombinase cassette (pSLG033) (Table S1). Using this mobilization-capable strain, we induced FLP recombinase with 4 mM arabinose and incubated cultures at 37 °C for 8 h. With primers flanking each of the seven genomic FRT sites (one unique to RTv2 and one unique to the genomic locus), we amplified the recombined genomic DNA from SQ171(pSLG022, pSLG033) (Figure 1b). Further study of a range of arabinose-induction conditions found robust induction of FLP activity in all conditions tested between 1 and 8 mM arabinose induction (Figure S1). We found that, across induced populations of this strain, DNA encoding RTv2 was integrated into each of the seven loci flanked by FRT sites

## a. Functional classes of FRT junctions on the FRT-junction map



## b. Mobilization of SQ171(pSLG022, pSLG033)

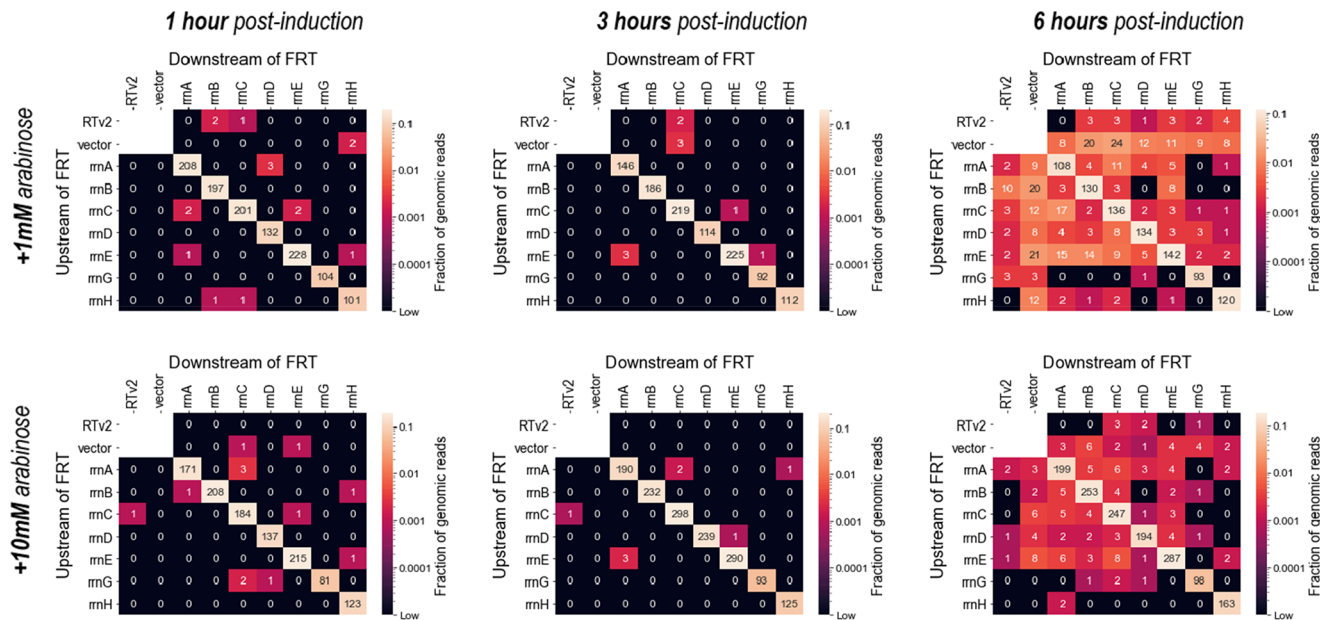


**Figure 2.** Dynamics of mobilized SQ171. (a) Schematic of the FRT-junction map showing functional classes and examples of FRT junctions in this experiment. (b) FRT-junction maps generated from NGS data on genome extractions of SQ171(pSLG022, pSLG033) cells mobilized with 1 mM arabinose and 10 mM arabinose for 1, 3, and 6 h. Each map is indexed by upstream-of-FRT and downstream-of-FRT regions corresponding to the two plasmid-based FRT-flanked cassettes (“RTv2” and “vector”) and to the seven genomic sites (“rrmA”–“rrmH”). In each map, the number of reads identified with each possible pair of upstream-of-FRT and downstream-of-FRT regions is shown. FRT junctions identified without at least one genomic index ( $2 \times 2$  area in the top left corner) have been excluded to focus analysis on genomic sites. The fraction of edited, or non-native, genomic FRT junctions compared to all FRT junctions calculated from each map is shown in Table 1 (here, native junctions are defined as the diagonal running from [rrmA, rrmA] to [rrmH, rrmH] and edited junctions are defined as all other sites shown). A simultaneous dilution plating experiment approximated the lethality of each condition compared to an uninduced control condition (Table 1). The fraction of edited junctions and the lethality rate were used to calculate estimated edits/mL/OD in viable cells for each condition. Under the optimal conditions shown here (1 mM arabinose for 6 h), the plasmid-borne mobilization system in SQ171(pSLG022, pSLG033) can generate approximately 11 million large (>5 kb) structural genomic edits per milliliter per OD in viable cells.

on the genome, confirmed by Sanger sequencing. We did not observe recombination without arabinose induction.

We then isolated clonal populations of SQ171(pSLG022, pSLG033) induced with a range of arabinose concentrations to evaluate the variability of integration of the RTv2 cassette across the seven loci. We performed colony PCR with primers flanking the seven genomic FRT sites and found that each clonal isolate has a characteristically different pattern of integration of the pSLG022 plasmid across the seven genomic FRT sites when compared to others isolated from the same population (Figure 1c). Thus, mobilization allows the independent generation of a unique set of structural genomic edits in each of the millions of *E. coli* contained within a single culture tube. Among the clones assayed, higher levels of arabinose induction did not appear to correlate strongly with higher amounts of recombination into target sites.

We next wanted to calibrate our mobilization strategy by finding conditions of arabinose induction and time of selection that produced a high number of genomic edits in viable cells. To do this, we grew SQ171(pSLG022, pSLG033) cells in liquid media and induced them with 0, 1, and 10 mM arabinose at  $OD_{600} \approx 0.1$ . After an induction period of 1, 3, and 6 h for each induction condition, fractions of cell culture from each condition were simultaneously genome-extracted for paired-end, next-generation sequencing (NGS), and dilution-plated on Luria–Bertani (LB) agar. To evaluate the data, we used a custom-built computational analysis pipeline that scans NGS read pairs for internal FRT sites, classifies the upstream-of-FRT and downstream-of-FRT-flanking regions in each read pair identified as having an internal FRT site, and records the resulting pair of classified FRT-flanking regions (Figure 2a).

Table 1. Calculated Values from FRT-Junction Mapping and Corresponding Lethality Experiment<sup>a</sup>

	value	1 h	3 h	6 h
1 mM arabinose	fraction of edited junctions	0.014	0.009	0.292
	lethality compared to uninduced control	0.417	0.435	0.983
	estimated edits/mL/OD in viable cells	$2.39 \times 10^6$	$1.19 \times 10^6$	$1.11 \times 10^7$
10 mM arabinose	fraction of edited junctions	0.012	0.005	0.087
	lethality compared to uninduced control	0.493	0.103	0.999
	estimated edits/mL/OD in viable cells	$1.64 \times 10^6$	$7.79 \times 10^6$	$7.73 \times 10^4$

<sup>a</sup>Fraction of edited junctions and lethality compared to uninduced control were used for each condition to calculate an estimated edits/mL/OD in viable cells. All dilution plates contributing colony counts to these data contained between 40 and 400 colonies.

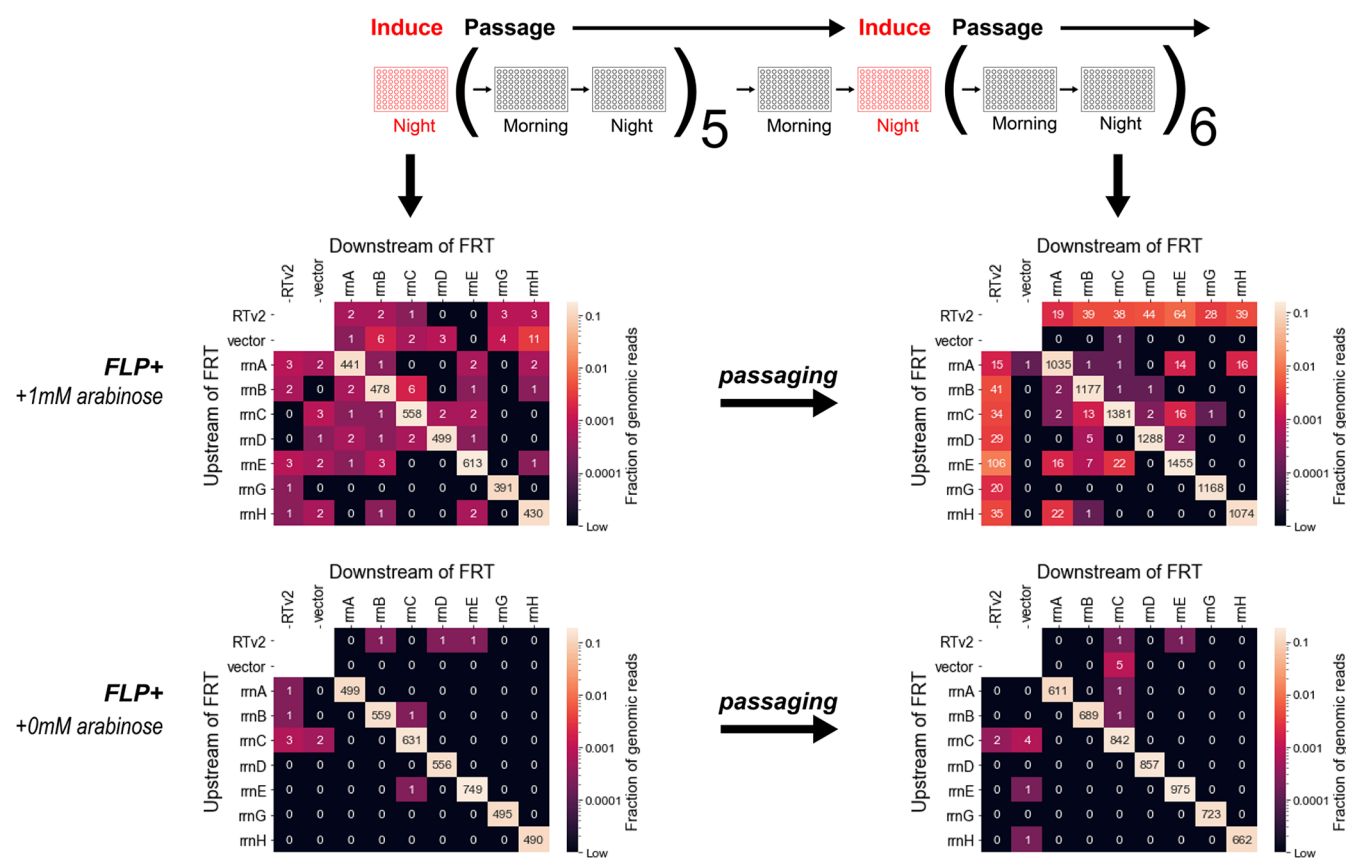


**Figure 3.** FLP-catalyzed evolution of genomic libraries toward genome-integrated-RTv2 genotypes. Passaging scheme and pooled FRT-junction maps for starting-point and ending-point samples induced with 1 mM arabinose or not induced with arabinose. Cultures were independently passaged twice daily in a 96-well plate in replicates of six for each condition. FLP+ denotes the presence of the arabinose-inducible FLP cassette in these cultures. Cultures were induced twice over the two-week passaging period by inoculation into culture media containing a gradient of arabinose (red plates); FRT-junction maps show starting point (after the first induction, left) and ending point (after complete passaging, right) cultures for all six replicates of the (FLP+, 0 mM arabinose) and (FLP+, 1 mM arabinose) conditions pooled together. As in Figure 2, FRT junctions not containing at least one native genomic FRT site have been hidden.

From this analysis, we constructed FRT-junction maps that profile relative quantities of FLP-FRT recombination events present in each condition (Figures 2b and S2). Relatively few FLP-mediated structural genomic edits occur before 6 h after induction in both 1 and 10 mM arabinose conditions, and lethality rates remain relatively low (Table 1). After 6 hours, large numbers of structural edits can be seen in both conditions, and lethality rates rise dramatically. The observed nonlinear FLP activity over time may be caused by the cooperative behavior of FLP recombinase:<sup>42</sup> as recombination is catalyzed by a tetrameric FLP complex joining two FRT sites, the number of FLP-mediated recombination events catalyzed per time responds sigmoidally to FLP concentration. In the 10 mM-arabinose conditions, the shock of many

recombination events appears to have caused a rapid die-off of these cells, resulting in a lethality rate of 99.9%. By comparison, in the 1 mM arabinose condition, the amount of FLP activity observed is appreciable for genomic library generation but not nearly as lethal. Under the best condition observed—6 h of induction with 1 mM arabinose—we calculated that the plasmid-borne mobilization system in SQ171(pSLG022, pSLG033) can generate approximately 11 million large (>5 kb) genomic insertions/deletions/rearrangements (structural edits) per milliliter per OD in viable cells (Table 1).

Under the 1 mM arabinose/6 h conditions, we observed evidence of widespread integration of the RTv2 cassette and the plasmid vector cassette into most available genomic sites (shown by the first row and column and second row and

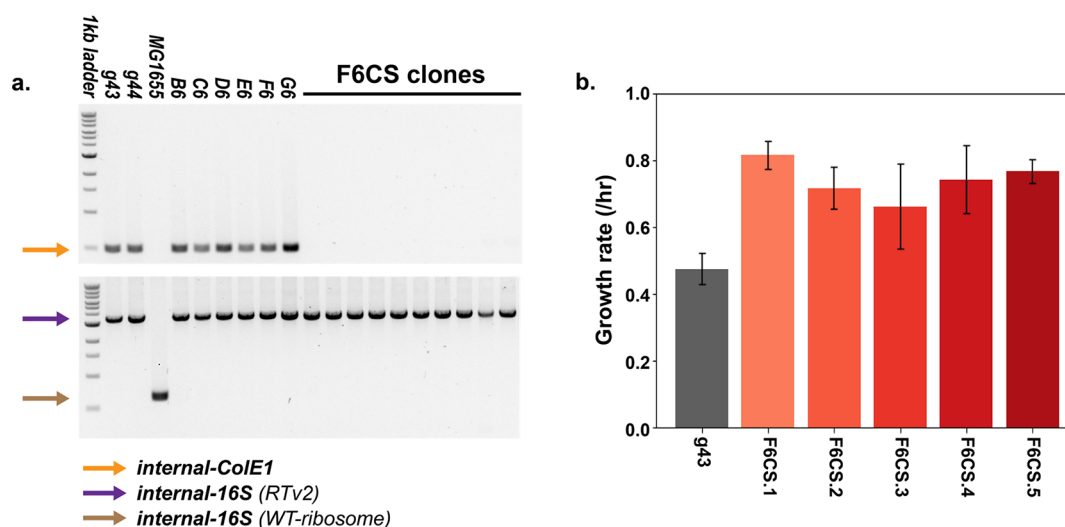


**Figure 4.** Characterization of population F6 clones after sucrose counterselection (F6CS clones). (a) Colony PCR reactions assaying for the presence of the ColE1 plasmid vector used in pSLG022 (top, orange arrow) and across the 16S rRNA (16S) of the small ribosomal subunit (bottom). g43 is the ancestral SQ171(pSLG022, pSLG033) strain; g44 is the ancestral SQ171(pSLG022, pSLG028) strain; MG1655 is a reference strain of wild-type *E. coli*; B6–G6 are the six 1 mM-arabinose pulse-passaged replicates evolved from g43 before sucrose counterselection. The 16S rRNA PCR produces products of different lengths when amplified from WT ribosomal operons (brown arrow) compared to RTv2 (purple arrow), which is because the tethered ribosome has circularly permuted 23S rRNA inserted into the 16S rRNA. (b) Comparison of growth rates of sucrose-counter-selected product clones (red shades) with their evolutionary ancestor strain (gray). Data are shown for  $n = 4$  or  $n = 5$  independent experiments with standard deviation for error. Full kinetic data with fitted model curves are shown in Figure S7.

column of each FRT-junction map, respectively), as well as rearrangements of portions of the genome. Genomic integrations of the plasmid vector seem to initially appear at higher rates than the RTv2 cassette. Additionally, genomic rearrangements may be biased toward rearrangements of smaller regions or between nearby FRT sites: in the base strain, *rrnC*, *rrnA*, *rrnB*, and *rrnE* FRT sites are all contained within a 250 kbp genomic segment, and recombination events between these sites appear to occur relatively frequently compared to those between other genomic sites. These observations demonstrate that mobilization is capable of rapidly exploring structural genomic space about both targeted FRT-flanked cassettes as well as rearrangements of large portions of the genome.

With our optimized mobilization strategy, we next wanted to use a laboratory evolution approach to evolve highly fit, genomically integrated-RTv2-dependent strains of *E. coli*. To do this, we designed an induction scheme for the recombinase-pulse passaging experiment (Figures 3a and S3). We passaged 60 cultures, split between 30 FLP+ and 30 FLP−, independently in a 96-well plate. These cultures were induced with a gradient of arabinose (0, 0.001, 0.01, 0.1, and 1 mM) twice over the two-week passaging period, resulting in six replicates for each condition. Cultures were passaged twice daily in a 1:100 dilution from the previous culture to maintain exponential growth as the dominant phase of the passaging cultures.

Following our passaging scheme, we extracted genomic samples from 24 of these populations (all six replicates of [FLP+, 0 mM arabinose], [FLP+, 1 mM arabinose], [FLP−, 0 mM arabinose], and [FLP−, 1 mM arabinose]) before and after passaging and submitted them for NGS to generate FRT-junction maps (Figure 3b). In the initial 1 mM arabinose condition, many FRT-junction recombination events can be seen (Figure 3b). Notably, these data were generated from genome extraction of a culture outgrown from the original

induced culture (which was necessary to generate enough material for genome extraction). As such, what appears to be a less diverse library shown in Figure 3b than generated from similar conditions in Figure 2 may be a result of several generations of selection having occurred between initial library generation and extraction. After the passaging period, genomic integrations of RTv2 cassette in the induced FLP+ condition are strongly enriched at each possible genomic site compared to their initial condition. At the same time, genomic integrations of the plasmid vector in the induced FLP+ condition, while being present at a similar rate as RTv2 integrations in the initial library, are significantly de-enriched after passaging. These data demonstrate that expression of RTv2 integrated onto the genome without the need of its original plasmid vector can have fitness benefits for the cell and therefore can be selected for through serial passaging. Additionally, certain genome restructuring events (e.g., formation of new junctions between former *rrnC* and *rrnE* genomic sites) appear to have been enriched in these final populations.

We observed that, of 551 total RTv2 genomic integrations found in the six [FLP+, 1 mM arabinose] populations, 509 (92.4%) occurred in the population found in well F6 (“population F6”), even though each of these populations was derived from one of six original replicates (Figure S3). That is, each population was treated with the same passaging and arabinose-induction conditions but was allowed to evolve independently. After plating F6 cultures on sucrose for counterselection of the pSLG022 vector, subsequent diagnostic PCRs show successful isolation of clones in which RTv2 is the dominant ribosomal population but which contain no ColE1-based plasmid vector (Figure 4a). Further PCR assays on a set of 19 isolated product clones are consistent with all clones containing a highly similar integration pattern of the RTv2 cassette at the *rrnC* and *rrnG* genomic sites and nowhere else among the assayed sites (Figure S4). Although the counter-

selection appears to have bottlenecked the diversity seen in the original F6 population, the resulting clones are now fully weaned from dependence upon plasmid-expressed RTv2.

Further characterization of five clones from the F6 population shows significantly higher growth rates than their evolutionary ancestor strain, with strain F6CS.1 growing ~71% faster than its ancestral strain (Figure 4b). Additionally, genome sequencing and subsequent analysis with the *breseq* package<sup>43</sup> confirmed loss of the plasmid vector and identified junctions between RTv2 and the reference genome at *rrnC* and *rrnG* as well as junctions with itself (as in a tandem array), with no other identified RTv2 junction sites (Tables S2 and S3). Coverage of the RTv2 cassette is between 17 and 25 times the coverage of average genomic sites, resulting in a putative genomic RTv2 copy number of 17–25 for these strains, which suggests that the RTv2 cassette may be clustered in repeats at either or both the *rrnC* and *rrnG* integration sites (Figure S6 and Table S3).

We next wanted to investigate the capacity for remobilization of the F6 strains living solely on genomically integrated RTv2 to understand whether mobilization was possible without assistance from FRT-containing episomal elements. We employed a second mobilization experiment using the F6CS.3 strain which resulted in significantly less lethality while still exhibiting recombination events at similar fractions of FRT junctions when compared to the plasmid-borne mobilization system, resulting in ~400 million edits/mL/OD in viable cells (Figure S5 and Table S4).

## DISCUSSION

In this work, we developed a FLP-recombinase-dependent mobilization system, which we demonstrate for the evolution of strains dependent on restructured, genomically expressed RTv2 as the cell-supporting ribosome population. By introduction of an RTv2 cassette flanked by two parallel FRT sites into *E. coli* and subsequent generation of genomic libraries via the stochastic action of FLP recombinase, we surveyed the landscape of possible solutions for a restructured, genomically expressed RTv2 strain at an approximate rate of 11 million edits per milliliter per OD in living cells of *E. coli* culture induced with 1 mM arabinose. After 2 weeks of serial passaging and subsequent counterselection of the plasmid vector, we isolated clonal strains dependent on genomically expressed tethered ribosomes as their sole ribosomal population. The F6CS strains show a marked increase in growth rate compared to their ancestral strain while containing a similar number of copies of the tethered ribosome cassette, demonstrating the power of mobilization to fine-tune the expression of Ribo-T-v2 in the context of the cellular translation machinery. Furthermore, we demonstrated that F6CS strains can be remobilized without an FRT-containing plasmid.

Given their improved growth characteristics and their less restricted episomal space, we expect that the F6CS strains generated here will be useful chassis for further ribosome and translation engineering. That said, several improvements to the mobilization protocol might be made to improve its versatility and targetability. The use of nondirectional target recombination sites, such as the *loxP* sites used in SCRaMble,<sup>38</sup> instead of directional FRT sites, would allow sequence inversions in addition to duplications or deletions and could provide another means for a mobilized cell to fine-tune the expression of the mobilized cassette. Additionally, the Cre/

LoxP recombination system could offer an alternative site-specific recombination system to FLP/FRT recombination. Furthermore, multiplexed automated genome engineering or no-scar recombineering might be useful for inserting or deactivating/deleting targeted FRT sites over the course of a mobilization experiment or after desired genome engineering is complete in order to produce an FRT-less strain.<sup>44,45</sup> Finally, high-throughput automation and selection could expand the power of mobilization to generate effective functional phenotypes.

One important consideration for future application of F6CS strains is genome stability. While we expect that most genome instability present during mobilization can be removed via removal/inactivation of the FLP recombinase gene, homology between FRT sites and duplicated RTv2 cassettes are another source of potential genome instability. Given that our primary goal was to build more robust and faster-growing strains dependent upon RTv2 as the cell's translating ribosome, any remaining genome instability that, for instance, results in duplication, inactivation, or deletion of RTv2 cassettes would be subject to continued selection pressure for faster growth and so would likely stay in line with that goal. However, in addition to the need for fast-growing, robust chassis strains, certain experiments and production processes that use living cells rely on genomic stability to ensure controlled conditions. Characterization of the genomic stability of F6CS strains could be important to include when planning such future work.

Looking forward, we imagine the F6CS strains' most immediate application being in the evolution of orthogonal ribosomes toward new functions *in vivo*, enabled by the increased growth rates and freed-up episomal space of F6CS strains compared to their predecessor strains based upon SQ171. For example, we expect that F6CS strains have a better capacity to support plasmid-based libraries of an orthogonal ribosome and subsequently allow a robust selection leveraged upon those orthogonal ribosome libraries via survival or fluorescence.

Additionally, we expect that mobilization could help build more complex synthetic translation systems, especially complex orthogonal translation systems with multiple orthogonal components. In this context, the combination of rich sequencing data generated from mobilization experiments and machine learning may help elucidate key cellular design principles for predicting how genomic architectures facilitate efficient synthetic translation systems. To this end, more powerful computational tools that incorporate understanding of the mechanisms of mobilization as well as experimental methods such as long-read sequencing could lead to powerful insights into evolutionary fitness and dynamics of complex genetic motifs within synthetic translation systems.

Finally, we hope that mobilization can be generalized for the construction and study of a variety of complex biological systems beyond the translation system in *E. coli*. While SQ171 has worked well for mobilization here with its seven native FRT sites, many other strains relevant for the study of various biological networks already possess one or more FRT sites as a product of historical genomic edits. If desired, additional FRT sites could easily be introduced at genomic locations of interest by a single researcher within weeks, thus generating suitable starting strains for mobilization. Ultimately, we look forward to mobilization's use as a flexible, powerful tool for studying and optimizing complex synthetic biological networks.

## MATERIALS AND METHODS

**Plasmid Construction and Exchange into SQ171.** The pSLG022 plasmid was constructed using Golden Gate assembly using the POP2136 strain, and the pSLG033 and pSLG028 plasmids were constructed using Gibson assembly. Sequence-verified constructs were transformed into SQ171 containing pRibo-T-v2 and ptRNA67<sup>31,41</sup> using electroporation and plated on their respective antibiotics to replace the previous resident plasmid: pSLG022 (kanamycin resistance) replaced pRibo-T-v2 (carbenicillin resistance), and pSLG033/pSLG028 (chloramphenicol resistance) replaced ptRNA67 (spectinomycin resistance). Transformed cells were screened against the resistance marker of the previous plasmid to ensure the loss of the former plasmid from the resulting colony. Previously used strains and references are shown in Table S7.

**Colony PCR Screening.** We screened cultures with colony PCR reactions to detect FLP-mediated recombination events at each former ribosomal operon site in SQ171. Specifically, forward primers were designed to bind plasmid-borne cassettes at the 3'-region of the FRT-flanked region containing Ribo-T-v2 or the plasmid vector from pSLG022, and reverse primers were designed to bind genomic sites downstream of each FRT scar that replaces a ribosomal operon site in SQ171 (Tables S5 and S6).

Colony PCR reactions were typically performed by inoculating 42.5 nL of liquid culture using an Echo550 pipetting system directly into a 10  $\mu$ L NEB Phusion high-fidelity DNA polymerase PCR mix. The reaction mix also contained 0.2 mM dNTPs and 0.2  $\mu$ M of each primer. PCRs were run using a modified touchdown PCR method:<sup>46</sup> initial denaturation at 98 °C for 5 min, 15 cycles of denaturation at 98 °C for 1 min, annealing at 72  $\rightarrow$  58 °C (subtracting 1 °C per cycle) for 1 min, and extension at 72 °C for 4 min, followed by 15 cycles of denaturation at 98 °C for 1 min, annealing at 57 °C for 1 min, and extension at 72 °C for 4 min, then a final extension at 72 °C for 10 min and holding at 12 °C. The resulting PCR products were loaded into a 1% agarose gel with SYBR Safe gel stain and run at 100 V for approximately 45 min. Each PCR product was also sequence-verified using Sanger sequencing.

**Lethality Assays.** To test the effect of FLP induction on cell viability, we grew cultures in LB + varying concentrations of arabinose. Cells were either inoculated into arabinose-containing media or induced with arabinose at OD  $\approx$  0.1. After a cell growth period of 1–6 h, cells were dilution-plated onto LB agar and grown at 37 °C until the formation of visible colonies. From dilution plates, colony counts were obtained from plates showing between 40 and 400 colonies. From these counts, expected CFU/mL/OD values were calculated, and the ratio of CFU/mL/OD measurements from cultures induced with arabinose compared to a noninduced control was calculated as the lethality rate.

**Mobilization and Serial Passaging.** We followed a “recombinase pulse-passaging” strategy in which a starting mobilizable system (pSLG022 + pSLG033) was introduced into cells and induced for FLP expression; then, the resulting population was passaged continuously to allow fast-growing clones to outcompete slower-growing clones (Figure S3). Specifically, 30 independent cultures of SQ171(pSLG022, pSLG033) and 30 independent cultures of SQ171(pSLG022, pSLG028) were grown with 200  $\mu$ L of LB–Miller + 15  $\mu$ g/mL chloramphenicol using the central 60 wells of a Corning 96

Well Clear Polystyrene Microplate (CLS3370). Each cell culture was induced on a gradient of 0  $\mu$ M arabinose, 1  $\mu$ M arabinose, 10  $\mu$ M arabinose, 100  $\mu$ M arabinose, and 1 mM arabinose in six replicates for a total of 30 independent cultures for each starting culture. Arabinose was added to the culture media before inoculation from the previous liquid culture. Cultures were passaged twice per day by inoculating 2  $\mu$ L of the previous day's culture into 200  $\mu$ L of fresh LB–Miller + 15  $\mu$ g/mL chloramphenicol.

**Vector Counterselection.** To remove the FRT-flanked vector cassette (SacB-KanR-CoIE1) from passaged cells able to live only off RTv2 expressed from the genome, promising cell populations identified by NGS screening were plated on LB-agar + 5% sucrose. The resulting colonies were then replica plated on LB-agar + 50  $\mu$ g/mL kanamycin to ensure pSLG022 vector loss. Colonies able to grow on the sucrose-containing media but susceptible to the kanamycin-containing media were outgrown in LB–Miller + 5% sucrose and then plated again on LB agar + 5% sucrose. This passaging and plating in the sucrose-containing-medium step was repeated at least once to ensure resulting clonal purity.

**Growth Rate Characterization.** Growth rates of strains and populations were measured in four or five replicates in a plate reader in Corning 96-well or 384-well clear polystyrene microplates. Growth rates were determined by fitting a linear regression to a plot of natural-log-transformed OD<sub>600</sub> readings as a function of time. Before curve fitting, the background signal of blank medium-containing wells was subtracted from raw measured OD<sub>600</sub> values. The curve-fitting algorithm finds the linear regression over a subsection of the curve corresponding to a 2–5 h time window with the highest R<sup>2</sup> value that spans at least 1.5 orders of magnitude of the log-transformed OD<sub>600</sub> data. The slope of this best-fitting linear regression is interpreted as the growth rate of the culture. Growth rates for each of the four or five replicates are then averaged and plotted with error bars as standard deviations.

**NGS Sample Preparation and FRT-Junction Map Analysis.** To build FRT-junction maps, sample libraries were prepared for NGS from genome extractions using the Invitrogen PureLink Genomic DNA Mini Kit. Genome extractions were fragmented to a target size of  $\sim$ 700 bp and then prepared for analysis on an Illumina platform with paired-end reads using the NEBNext Ultra II DNA Library Prep Kit.

To analyze the resulting dataset, a computational pipeline was built in the iPython environment (Jupyter notebooks), using the Biopython package to assist alignment functions.<sup>47</sup> In brief, for each sample, paired-end-read pairs were analyzed by pairwise local alignment to the 34-bp FRT sequence (“forward” direction: GAAGTTCCTATTCTCTAGAAAG-TATAGGAACTTC, “reverse” direction: GAAGTTCCTA-TACTTTCTAGAGAATAGGAACTTC). Additionally, each read was independently aligned to known upstream and downstream sequences of FRT sites to determine whether a putative, nonsequenced FRT site may exist on the fragment between sequenced read pairs. In either case, those read pairs with an identified putative internal FRT site were selected for further analysis.

The location of the putative FRT site was used to determine putative upstream-of-FRT and downstream-of-FRT regions within the read pair. Given that FRT sites are directional, upstream-of-FRT and downstream-of-FRT sequence sets are expected to remain constant without switching independent of the FRT-mediated recombination events that have occurred in

a strain (e.g., a site that is immediately upstream of an FRT site is expected to remain upstream of an FRT site, although its downstream partner may change). Therefore, the upstream-of-FRT and downstream-of-FRT sequences from each read pair with a putative internal FRT site were aligned to the sets of known upstream-of-FRT and downstream-of-FRT sequences, respectively, to determine putative identities for the upstream-of-FRT and downstream-of-FRT sequences. Sequences returning an alignment score that is both  $\geq 50$  (match score: 1; mismatch score:  $-1.25$ ; open gap score:  $-5$ ; extend gap score:  $-1$ ) and a ratio of 1.4 higher than the next-highest alignment score from the set of possible alignments were considered positively identified. Upstream or downstream regions unable to pass these criteria were classified as “not identified”.

This alignment is done for both the upstream-of-FRT and downstream-of-FRT regions from the paired-end reads to generate an index pair that uniquely classifies the analyzed FRT junction as one of 81 possible types (plus 19 additional possible junctions where one or both junctions are not able to be identified). The set of index pairs for sequenced FRT junctions was used to construct resulting FRT-junction maps for each strain or population analyzed, with each identified index pair generated from one read pair adding one count to its box in the resulting FRT-junction map.

**breseq Analysis.** The *breseq* package from the Barrick lab<sup>43</sup> was run on an Ubuntu installation on paired-end reads generated from next-generation Illumina sequencing pipelines, using both the SQ171 genome and the pSLG022 plasmid map as reference sequences simultaneously (Table S1).

**Editing Rate Analysis.** To approximate the FLP/FRT-mediated editing rate across a strain population, SQ171-(pSLG022, pSLG033) cultures were induced with arabinose at  $OD \approx 0.1$ , then subsamples were periodically measured for  $OD_{600}$  absorbance, dilution-plated, and genome-extracted for submission to NGS. Using the resulting datasets, we calculated an approximate number of recombination events caused by FLP (edits) per culture volume using the following equation:

$$\frac{\text{edits in viable cells}}{\text{mL} \times \text{OD}} = \frac{\text{edited FRT}}{\text{total FRT}} \times \frac{\text{FRT}}{\text{cell}} \times \frac{\text{expected cells}}{\text{mL} \times \text{OD}} \times \text{survival rate}$$

where edited FRT is defined as the total counts of genomic junctions in an FRT-junction map excluding those native to the starting strain, and total FRT includes all counts of genomic junctions. In the plasmid-borne system, this encompasses all FRT sites counted excluding the native FRT junctions at *rrnA*, *rrnB*, *rrnC*, *rrnD*, *rrnE*, *rrnG*, and *rrnH*. For the genome-bound system, the native FRT junctions include *rrnA*, *rrnB*, *rrnD*, *rrnE*, and *rrnH*, but the *rrnC* and *rrnG* junctions are replaced with corresponding RTv2 junctions at these sites. The edited-to-total FRT ratio of an uninduced control strain at each time point was subtracted from the same ratio for induced strains to account for the low rate of background recombinations seen in FRT-junction maps. FRT/cell is a constant defined by the number of unique genomic FRT sites expected in the initial system: 7 for the plasmid-borne system and 9 for the genome-bound system. Expected cells/mL/OD was calculated at each time point from dilution plating of a control strain that did not receive arabinose induction. Finally, the survival rate term is deduced from a corresponding lethality experiment by taking the ratio of CFU/

mL/OD from induced and uninduced samples at a given time point. This survival rate is equal to 1 minus lethality rates reported in Tables 1 and S4.

## ■ ASSOCIATED CONTENT

### Supporting Information

The Supporting Information is available free of charge at <https://pubs.acs.org/doi/10.1021/acssynbio.2c00099>.

Colony PCR screening of arabinose-induction conditions for relevant starting strains; unredacted FRT-junction maps from the experiment shown in Figure 2b; overall scheme of the pulse-passaging strategy; colony PCR screening of F6CS clones; FRT-junction maps and lethality experiment data generated from the mobilization of F6CS.3; example coverage map of an F6CS strain generated from *breseq*; raw kinetic growth data and individual calculated fits for the growth rate data shown in Figure 4b; plasmid maps and sequences; *breseq*-generated new junction evidence for F6CS.1 genomic extractions; individual mean coverage and RTv2 copy number estimations for strains F6CS.1-5; and primer and strain sequences and information (PDF)

## ■ AUTHOR INFORMATION

### Corresponding Author

Michael C. Jewett – Department of Chemical and Biological Engineering, Northwestern University, Evanston, Illinois 60208, United States; Chemistry of Life Processes Institute and Center for Synthetic Biology, Northwestern University, Evanston, Illinois 60208, United States; Simpson Querrey Institute, Northwestern University, Chicago, Illinois 60611, United States; [orcid.org/0000-0003-2948-6211](https://orcid.org/0000-0003-2948-6211); Phone: (+1) 847 467 5007; Email: [m-jewett@northwestern.edu](mailto:m-jewett@northwestern.edu); Fax: (+1) 847 491 3728

### Author

Samuel Gowland – Department of Chemical and Biological Engineering, Northwestern University, Evanston, Illinois 60208, United States; Chemistry of Life Processes Institute, Northwestern University, Evanston, Illinois 60208, United States

Complete contact information is available at:

<https://pubs.acs.org/doi/10.1021/acssynbio.2c00099>

### Author Contributions

S.G. and M.C.J. conceived the study, designed experiments, and wrote the paper. S.G. carried out the experiments and analyzed the data.

### Notes

The authors declare the following competing financial interest(s): M.C.J. has a financial interest in Pearl Bio. M.C.J.'s interests are reviewed and managed by Northwestern University in accordance with their conflict-of-interest policies. All other authors declare no conflicts of interest.

The authors declare that all NGS data supporting the findings in this study have been deposited at the National Center for Biotechnology Information (NCBI) Sequence Read Archive, with BioProject ID PRJNA853475, accessible at <https://www.ncbi.nlm.nih.gov/sra/PRJNA853475>. All other experimental data supporting the findings of this study are available within the paper and its supplementary files. All data related to models are available upon request from the authors.

## ACKNOWLEDGMENTS

This work was supported by the National Science Foundation (MCB-1716766), the Human Frontiers Science Program (RGP0015/2017), and Army Contracting Command (W52P1J-21-9-3023). S.G. was supported in part by the National Institutes of Health Training Grant (T32GM008449) through Northwestern University's Biotechnology Training Program. The U.S. Government is authorized to reproduce and distribute reprints for Governmental purposes notwithstanding any copyright notation thereon. The views and conclusions contained herein are those of the authors and should not be interpreted as necessarily representing the official policies or endorsements, either expressed or implied, of the U.S. Government.

## REFERENCES

- (1) Kofman, C.; Lee, J.; Jewett, M. C. Engineering molecular translation systems. *Cell Syst.* **2021**, *12*, 593–607.
- (2) O'Donoghue, P.; Ling, J.; Wang, Y.-S.; Söll, D. Upgrading protein synthesis for synthetic biology. *Nat. Chem. Biol.* **2013**, *9*, 594–598.
- (3) Chin, J. W. Expanding and reprogramming the genetic code. *Nature* **2017**, *550*, 53–60.
- (4) Hammerling, M. J.; Krüger, A.; Jewett, M. C. Strategies for in vitro engineering of the translation machinery. *Nucleic Acids Res.* **2019**, *48*, 1068–1083.
- (5) Des Soye, B. J.; Patel, J. R.; Isaacs, F. J.; Jewett, M. C. Repurposing the translation apparatus for synthetic biology. *Curr. Opin. Chem. Biol.* **2015**, *28*, 83–90.
- (6) Katoh, T.; Sengoku, T.; Hirata, K.; Ogata, K.; Suga, H. Ribosomal synthesis and de novo discovery of bioactive foldamer peptides containing cyclic  $\beta$ -amino acids. *Nat. Chem.* **2020**, *12*, 1081–1088.
- (7) Katoh, T.; Suga, H. Ribosomal Incorporation of Consecutive  $\beta$ -Amino Acids. *J. Am. Chem. Soc.* **2018**, *140*, 12159–12167.
- (8) Katoh, T.; Suga, H. Ribosomal Elongation of Cyclic  $\gamma$ -Amino Acids using a Reprogrammed Genetic Code. *J. Am. Chem. Soc.* **2020**, *142*, 4965–4969.
- (9) Katoh, T.; Tajima, K.; Suga, H. Consecutive Elongation of D-Amino Acids in Translation. *Cell Chem. Biol.* **2017**, *24*, 46–54.
- (10) Fujino, T.; Goto, Y.; Suga, H.; Murakami, H. Ribosomal Synthesis of Peptides with Multiple  $\beta$ -Amino Acids. *J. Am. Chem. Soc.* **2016**, *138*, 1962–1969.
- (11) Lee, J.; Schwarz, K. J.; Kim, D. S.; Moore, J. S.; Jewett, M. C. Ribosome-mediated polymerization of long chain carbon and cyclic amino acids into peptides in vitro. *Nat. Commun.* **2020**, *11*, 4304.
- (12) Lee, J.; Schwarz, K. J.; Yu, H.; Krüger, A.; Anslyn, E. V.; Ellington, A. D.; Moore, J. S.; Jewett, M. C. Ribosome-mediated incorporation of fluorescent amino acids into peptides in vitro. *Chem. Commun.* **2021**, *57*, 2661–2664.
- (13) Lee, J.; Torres, R.; Kim, D. S.; Byrom, M.; Ellington, A. D.; Jewett, M. C. Ribosomal incorporation of cyclic  $\beta$ -amino acids into peptides using in vitro translation. *Chem. Commun.* **2020**, *56*, 5597–5600.
- (14) Lee, J.; Schwieter, K. E.; Watkins, A. M.; Kim, D. S.; Yu, H.; Schwarz, K. J.; Lim, J.; Coronado, J.; Byrom, M.; Anslyn, E. V.; Ellington, A. D.; Moore, J. S.; Jewett, M. C. Expanding the limits of the second genetic code with ribozymes. *Nat. Commun.* **2019**, *10*, 5097.
- (15) Rogers, J. M.; Kwon, S.; Dawson, S. J.; Mandal, P. K.; Suga, H.; Huc, I. Ribosomal synthesis and folding of peptide-helical aromatic foldamer hybrids. *Nat. Chem.* **2018**, *10*, 405–412.
- (16) Takatsui, R.; Shinbara, K.; Katoh, T.; Goto, Y.; Passioura, T.; Yajima, R.; Komatsu, Y.; Suga, H. Ribosomal Synthesis of Backbone-Cyclic Peptides Compatible with In Vitro Display. *J. Am. Chem. Soc.* **2019**, *141*, 2279–2287.
- (17) Kakkar, N.; Perez, J. G.; Liu, W. R.; Jewett, M. C.; van der Donk, W. A. Incorporation of Nonproteinogenic Amino Acids in Class I and II Lantibiotics. *ACS Chem. Biol.* **2018**, *13*, 951–957.
- (18) Yu, Y.; Zhou, Q.; Wang, L.; Liu, X.; Zhang, W.; Hu, M.; Dong, J.; Li, J.; Lv, X.; Ouyang, H.; Li, H.; Gao, F.; Gong, W.; Lu, Y.; Wang, J. Significant improvement of oxidase activity through the genetic incorporation of a redox-active unnatural amino acid. *Chem. Sci.* **2015**, *6*, 3881–3885.
- (19) Zimmerman, E. S.; Heibeck, T. H.; Gill, A.; Li, X.; Murray, C. J.; Madlansacay, M. R.; Tran, C.; Uter, N. T.; Yin, G.; Rivers, P. J.; Yam, A. Y.; Wang, W. D.; Steiner, A. R.; Bajad, S. U.; Penta, K.; Yang, W.; Hallam, T. J.; Thanos, C. D.; Sato, A. K. Production of Site-Specific Antibody-Drug Conjugates Using Optimized Non-Natural Amino Acids in a Cell-Free Expression System. *Bioconjugate Chem.* **2014**, *25*, 351–361.
- (20) Costa, S. A.; Mozhdzhi, D.; Dzuricky, M. J.; Isaacs, F. J.; Brustad, E. M.; Chilkoti, A. Active Targeting of Cancer Cells by Nanobody Decorated Polypeptide Micelle with Bio-orthogonally Conjugated Drug. *Nano Lett.* **2019**, *19*, 247–254.
- (21) Lajoie, M. J.; Rovner, A. J.; Goodman, D. B.; Aerni, H.-R.; Haimovich, A. D.; Kuznetsov, G.; Mercer, J. A.; Wang, H. H.; Carr, P. A.; Mosberg, J. A.; Rohland, N.; Schultz, P. G.; Jacobson, J. M.; Rinehart, J.; Church, G. M.; Isaacs, F. J. Genomically Recoded Organisms Expand Biological Functions. *Science* **2013**, *342*, 357–360.
- (22) Mandell, D. J.; Lajoie, M. J.; Mee, M. T.; Takeuchi, R.; Kuznetsov, G.; Norville, J. E.; Gregg, C. J.; Stoddard, B. L.; Church, G. M. Biocontainment of genetically modified organisms by synthetic protein design. *Nature* **2015**, *518*, 55–60.
- (23) Rovner, A. J.; Haimovich, A. D.; Katz, S. R.; Li, Z.; Grome, M. W.; Gassaway, B. M.; Amiram, M.; Patel, J. R.; Gallagher, R. R.; Rinehart, J.; Isaacs, F. J. Recoded organisms engineered to depend on synthetic amino acids. *Nature* **2015**, *518*, 89–93.
- (24) Fredens, J.; Wang, K.; de la Torre, D.; Funke, L. F. H.; Robertson, W. E.; Christova, Y.; Chia, T.; Schmied, W. H.; Dunkelmann, D. L.; Beránek, V.; Uttamapinant, C.; Llamazares, A. G.; Elliott, T. S.; Chin, J. W. Total synthesis of *Escherichia coli* with a recoded genome. *Nature* **2019**, *569*, 514–518.
- (25) Wang, K.; Fredens, J.; Brunner, S. F.; Kim, S. H.; Chia, T.; Chin, J. W. Defining synonymous codon compression schemes by genome recoding. *Nature* **2016**, *539*, 59–64.
- (26) Robertson, E.; Funke, F. H.; de la Torre, D.; Fredens, J.; Elliott, S.; Spinck, M.; Christova, Y.; Cervettini, D.; Böge, L.; Liu, C.; Buse, S.; Maslen, S.; Salmond, P. C.; Chin, W. Sense codon reassignment enables viral resistance and encoded polymer synthesis. *Science* **2021**, *372*, 1057–1062.
- (27) Aleksashin, N. A.; Leppik, M.; Hockenberry, A. J.; Klepacki, D.; Vázquez-Laslop, N.; Jewett, M. C.; Remme, J.; Mankin, A. S. Assembly and functionality of the ribosome with tethered subunits. *Nat. Commun.* **2019**, *10*, 930.
- (28) Yesselman, J. D.; Eiler, D.; Carlson, E. D.; Gotrik, M. R.; d'Aquino, A. E.; Ooms, A. N.; Kladwang, W.; Carlson, P. D.; Shi, X.; Costantino, D. A.; Herschlag, D.; Lucks, J. B.; Jewett, M. C.; Kieft, J. S.; Das, R. Computational design of three-dimensional RNA structure and function. *Nat. Nanotechnol.* **2019**, *14*, 866–873.
- (29) Aleksashin, N. A.; Szal, T.; d'Aquino, A. E.; Jewett, M. C.; Vázquez-Laslop, N.; Mankin, A. S. A fully orthogonal system for protein synthesis in bacterial cells. *Nat. Commun.* **2020**, *11*, 1858.
- (30) Orelle, C.; Carlson, E. D.; Szal, T.; Florin, T.; Jewett, M. C.; Mankin, A. S. Protein synthesis by ribosomes with tethered subunits. *Nature* **2015**, *524*, 119.
- (31) Carlson, E. D.; d'Aquino, A. E.; Kim, D. S.; Fulk, E. M.; Hoang, K.; Szal, T.; Mankin, A. S.; Jewett, M. C. Engineered ribosomes with tethered subunits for expanding biological function. *Nat. Commun.* **2019**, *10*, 3920.
- (32) Fried, S. D.; Schmied, W. H.; Uttamapinant, C.; Chin, J. W. Ribosome Subunit Stapling for Orthogonal Translation in *E. coli*. *Angew. Chem., Int. Ed.* **2015**, *54*, 12791–12794.
- (33) Kim, D. S.; Watkins, A.; Bidstrup, E.; Lee, J.; Topkar, V.; Schwarz, K. J.; Kofman, C.; Schwarz, K. J.; Liu, Y.; Pintilie, G.; Roney,

E.; Das, R.; Jewett, M. C. 3D-structure-guided evolution of a ribosome with tethered subunits. *Nat. Chem. Biol.* **2022**, DOI: 10.1038/s41589-022-01064-w. In press

(34) Datsenko, K. A.; Wanner, B. L. One-step inactivation of chromosomal genes in *Escherichia coli* K-12 using PCR products. *PNAS* **2000**, *97*, 6640–6645.

(35) Bassalo, M. C.; Garst, A. D.; Halweg-Edwards, A. L.; Grau, W. C.; Domaille, D. W.; Mutalik, V. K.; Arkin, A. P.; Gill, R. T. Rapid and Efficient One-Step Metabolic Pathway Integration in *E. coli*. *ACS Synth. Biol.* **2016**, *5*, 561–568.

(36) Des Soye, B. J.; Gerbasi, V. R.; Thomas, P. M.; Kelleher, N. L.; Jewett, M. C. A Highly Productive, One-Pot Cell-Free Protein Synthesis Platform Based on Genomically Recoded *Escherichia coli*. *Cell Chem. Biol.* **2019**, *26*, 1743–1754 e9.

(37) Ma, L.; Li, Y.; Chen, X.; Ding, M.; Wu, Y.; Yuan, Y.-J. SCRaMbLE generates evolved yeasts with increased alkali tolerance. *Microb. Cell Fact.* **2019**, *18*, 52.

(38) Dymond, J.; Boeke, J. The *Saccharomyces cerevisiae* SCRaMbLE system and genome minimization. *Bioeng. Bugs* **2012**, *3*, 168–171.

(39) Jia, B.; Wu, Y.; Li, B.-Z.; Mitchell, L. A.; Liu, H.; Pan, S.; Wang, J.; Zhang, H.-R.; Jia, N.; Li, B.; Shen, M.; Xie, Z.-X.; Liu, D.; Cao, Y.-X.; Li, X.; Zhou, X.; Qi, H.; Boeke, J. D.; Yuan, Y.-J. Precise control of SCRaMbLE in synthetic haploid and diploid yeast. *Nat. Commun.* **2018**, *9*, 1933.

(40) Luo, Z.; Wang, L.; Wang, Y.; Zhang, W.; Guo, Y.; Shen, Y.; Jiang, L.; Wu, Q.; Zhang, C.; Cai, Y.; Dai, J. Identifying and characterizing SCRaMbLEd synthetic yeast using ReSCuES. *Nat. Commun.* **2018**, *9*, 1930.

(41) Quan, S.; Skovgaard, O.; McLaughlin, R. E.; Buurman, E. T.; Squires, C. L. Markerless *Escherichia coli* *rrn* Deletion Strains for Genetic Determination of Ribosomal Binding Sites. *G3: Genes, Genomes, Genet.* **2015**, *5*, 2555–2557.

(42) Ringrose, L.; Lounnas, V.; Ehrlich, L.; Buchholz, F.; Wade, R.; Stewart, A. F. Comparative kinetic analysis of FLP and cre recombinases: mathematical models for DNA binding and recombination. *J. Mol. Biol.* **1998**, *284*, 363–384.

(43) Deatherage, D. E.; Barrick, J. E. Identification of mutations in laboratory-evolved microbes from next-generation sequencing data using breseq. *Methods Mol. Biol.* **2014**, *1151*, 165–188.

(44) Wang, H. H.; Isaacs, F. J.; Carr, P. A.; Sun, Z. Z.; Xu, G.; Forest, C. R.; Church, G. M. Programming cells by multiplex genome engineering and accelerated evolution. *Nature* **2009**, *460*, 894.

(45) Rangarajan, A. A.; Yilmaz, C.; Schnetz, K. Deletion of FRT-sites by no-SCAR recombineering in *Escherichia coli*. *Microbiology* **2022**, *168* (4), DOI: 10.1099/mic.0.001173.

(46) Korbie, D. J.; Mattick, J. S. Touchdown PCR for increased specificity and sensitivity in PCR amplification. *Nat. Protoc.* **2008**, *3*, 1452–1456.

(47) Cock, P. J. A.; Antao, T.; Chang, J. T.; Chapman, B. A.; Cox, C. J.; Dalke, A.; Friedberg, I.; Hamelryck, T.; Kauff, F.; Wilczynski, B.; de Hoon, M. J. L. Biopython: freely available Python tools for computational molecular biology and bioinformatics. *Bioinformatics* **2009**, *25*, 1422–1423.

## Recommended by ACS

### Standard Intein Gene Expression Ramps (SIGER) for Protein-Independent Expression Control

Maxime Fages-Lartaud, Martin Frank Hohmann-Marriott, *et al.*

MARCH 15, 2023

ACS SYNTHETIC BIOLOGY

[READ](#)

### Phage N15-Based Vectors for Gene Cloning and Expression in Bacteria and Mammalian Cells

Yin Cheng Wong, Kumaran Narayanan, *et al.*

APRIL 06, 2023

ACS SYNTHETIC BIOLOGY

[READ](#)

### Clonal Amplification-Enhanced Gene Expression in Synthetic Vesicles

Zhanar Abil, Christophe Danelon, *et al.*

APRIL 04, 2023

ACS SYNTHETIC BIOLOGY

[READ](#)

### Reconstitution of Multi-Protein Complexes through Ribozyme-Assisted Polycistronic Co-Expression

Yan Liu, Jinzhong Lin, *et al.*

DECEMBER 13, 2022

ACS SYNTHETIC BIOLOGY

[READ](#)

[Get More Suggestions >](#)